2017

Effects of span-to-depth ratios on moment connection damage evolution under catenary action

Ling Li
Tongji University, University of Wollongong

Wei Wang
Tongji University

Lip H. Teh
University of Wollongong, lteh@uow.edu.au

Yiyi Chen
Tongji University

Effects of span-to-depth ratios on moment connection damage evolution under catenary action

Abstract

This paper proposes an improved method for determining the gravity resistance of a moment resisting beam-column assembly following an interior column loss. The proposed method accounts for the connection's damage evolution and for the catenary mechanism developed by the assembly as it deflects downward. Through a full-scale laboratory test and finite element simulations, the complete responses of moment resisting beam-column assemblies including the connection's damage evolution are investigated under different beam span-to-depth ratios. The welded unreinforced flange-bolted web (WUF-BW) connection method is used for its robustness in developing the catenary action. It is found that, under the same span-to-depth ratio, beam-column assemblies exhibit similar normalized load-rotation relationships, even with different beam depths. The assembly with a larger span-to-depth ratio is able to develop the gravity resistance earlier, and provides a higher ultimate resistance by developing a more effective catenary mechanism. On the other hand, the assembly with a smaller span-to-depth ratio exhibits a more ductile response. A simplified curve model of the gravity resistance development of a moment beam-column assembly with damage evolution has been proposed for a convenient assessment of the progressive collapse resistance following a central column loss.

Disciplines

Engineering | Science and Technology Studies

Publication Details

Li, L., Wang, W., Teh, L. H. & Chen, Y. (2017). Effects of span-to-depth ratios on moment connection damage evolution under catenary action. Journal of Constructional Steel Research, 139 18-29.

This article was originally published as Li, L., Wang, W., Teh, L. H. & Chen, Y. (2017). Effects of span-to-depth ratios on moment connection damage evolution under catenary action. *Journal of Constructional Steel Research, 139 18-29.*

Effects of Span-to-Depth Ratios on Damage Evolution of Moment Connections in Column Removal Scenario

Ling Li [a, c], Wei Wang [a, b,]*, Lip H. Teh [c], Yiyi Chen [a, b]

[a] *State Key Laboratory of Disaster Reduction in Civil Engineering, Tongji University, Shanghai 200092, China*

[b] *Department of Structural Engineering, Tongji University, Shanghai 200092, China*

[c] *School of Civil, Mining and Environmental Engineering, University of Wollongong, Wollongong, NSW 2522, Australia*

Abstract: This paper proposes an improved method for determining the gravity resistance of a moment resisting beam-column assembly following an interior column loss. The proposed method accounts for the connection's damage evolution and for the catenary mechanism developed by the assembly as it deflects downward. Through a full-scale laboratory test and finite element simulations, the complete responses of moment resisting beam-column assemblies including the connection's damage evolution are investigated under different beam span-to-depth ratios. The welded unreinforced flange-bolted web (WUF-BW) connection method is used for its robustness in developing the catenary action. It is found that, under the same span-to-depth ratio, beam-column assemblies exhibit similar normalized load-rotation relationships, even with different beam depths. The assembly with a larger span-to-depth ratio is able to develop the gravity resistance earlier, and provides a higher ultimate resistance by developing a more effective catenary mechanism. On the other hand, the assembly with a smaller span-to-depth ratio exhibits a more ductile response. A simplified curve model of the gravity resistance development of a moment beam-column assembly with damage evolution has been proposed for a convenient assessment of the progressive collapse resistance following a central column loss.

Keywords: progressive collapse; span-to-depth ratio; steel moment connection; gravity resistance development; damage evolution; catenary mechanism; flexural mechanism.

---

* Corresponding author. Tel.: +86-21-65982926; Fax: +86-21-65984976.

Email address: weiwang@tongji.edu.cn (W. Wang)

1. Introduction

There have been several guidelines [1-3] for the progressive collapse design and analysis of building structures under extreme or abnormal load, all of which employ basically the same principles and analysis methods. According to UFC 4-023-03 "Design of building to resist progressive collapse" [2], a progressive collapse design may use different methods depending on the occupancy category of the building, including the Tie Force (TF) method for the entire structure, the Alternate Path (AP) method and the Enhanced Local Resistance (ELR) method for some specific structure regions.

The Alternate Path method [4], as both the design and the analysis methods, is the most popular for the study of progressive collapse prevention [1-3]. A structure must be able to bridge over vertical load-carrying elements notionally removed from itself by satisfying the requirements of the Alternate Path method, otherwise it must be re-designed or retrofitted to increase the structural bridging capacity [2, 3]. In this method, any further failure of structural components (connections, beams and columns) following the notional column removal is prevented by ensuring the components meet certain criteria for various building materials including reinforced concrete, structural steel, masonry and wood [2, 3].

It has been found [5-10] that the structural bridging capacity depends on the performance of the connections. There have been a number of experimental tests and numerical simulations focusing on the behaviour of various connections [11-21] following an interior column loss. The moment connections were found to work firstly by flexural action and later by catenary action [6, 14, 15, 18-20]. It was found [15, 18-21] that a steel moment connection usually acquires a meaningful contribution to the gravity resistance from the catenary mechanism at chord rotations greater than 0.03 radians.

When the nonlinear static analysis procedure is employed, nominally rigid moment connections must deform within the prescribed deformation limits so as to meet the acceptance criteria [2]. The acceptance criteria for moment connections are given in terms of the plastic rotation, whose values for a primary component correspond to its plastic deformation limit prior to capacity degradation [2-3]. Moment connections are permitted to deform within a small range of plastic rotations, below 0.025 radians for the typical "improved welded unreinforced flange-bolted web" (WUF-BW) connection [2, 3], which does not allow any significant catenary action to be developed [15, 18-22]. However, the capacity degradation does not usually occur until a much larger rotation, typically greater than 0.06 radians [15, 18-21].

In traditional seismic structural designs, the occurrence of fracture signifies the ultimate limit state of a moment connection due to the loss of its flexural capacity. However, in an interior column removal scenario, catenary action can still be developed by the tensioning of the connected beam members under large deflection following fracture, provided the connections are designed appropriately [18-22]. Two types of moment connection failure modes, being the beam-end interrupted failure mode and the column-wall failure mode, have been identified [18-20] as being able to allow the assembly to obtain a higher gravity resistance (from the catenary mechanism) in the post-fracture stage than its previous peak resistance (under the flexural mechanism). It is therefore rational to explore new design criteria that take advantage of the catenary mechanism that develops following an interior column loss.

Among the various levels of sub-structure idealisation in the simplified framework proposed by Izzuddin et al. [23] for multi-storey buildings, the double-span beam-column assembly within the bays above the lost column is the lowest level of sub-structure whose response is used for composing the higher level sub-structures. The beam's span-to-depth ratio has been found to significantly affect the response of the double-span beam-column assembly following the column removal [24-27]. However, these investigations did not account for the damage evolution of the beam-to-column connections.

In this paper, the complete responses of the moment resisting beam-column assemblies under the column removal scenario are investigated. The welded unreinforced flange-bolted web (WUF-BW) is used to connect the beams and the column as such a connection facilitates the development of the catenary mechanism following an initial fracture. The development of the assembly's gravity resistance in the post-fracture stage and the effects of the span-to-depth ratio are studied in detail.

A full-scale laboratory test is conducted where a pushdown action at the central column is applied in order to simulate the column removal scenario. The test results are used to verify the refined finite element model incorporating material fracture, which is employed in subsequent parametric analyses of the effects of the beam span-to-depth ratio on the gravity resistance of the beam-column assemblies. Based on the parametric analyses results, an improved development model will be proposed for the structural gravity resistance taking into account the damage evolution of the connection region.

2. Full-scale laboratory test

2.1. Test specimen

Due to its robustness during the beam-end interrupted failure and column-wall failure under a central column removal scenario [18, 19], the welded unreinforced flange-bolted web (WUF-BW) connection was used for the test specimen whose details are given in Fig. 1. The double-span assembly consisted of two I-section beams (H300×150×6×8) and a square hollow section column (SHS250×14) with two inner diaphragms (thickness t = 8mm) at locations corresponding to the top and the bottom flanges of the beam, as illustrated in Fig. 1 (b).

The flanges of the beam and the inner diaphragms were joined to the column wall using complete joint penetration (CJP) groove welds, and weld access holes of the beam were cut from the beam web in accordance with the standard recommendation [28]. The beam webs were bolted to the shear tab welded to the column via four M20 Grade 10.9 frictional type high-strength bolts arranged in one vertical row. The tightening torque applied on the bolts was 440 N-m according to standard requirements [29]. All the contact surfaces were treated with sand blasting. The measured material properties of the specimen are summarized in Table 1.

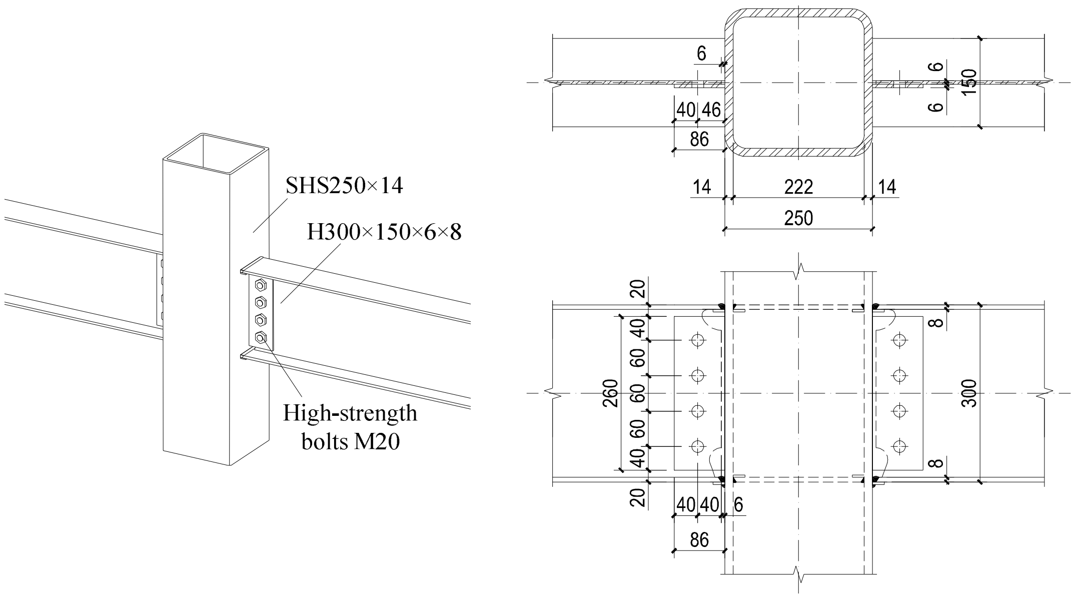

(a) Components. (b) Dimensions (in mm).

Fig. 1. Details of the WUF-BW connection.

Table 1. Material properties of test specimen.

Components	Yield strength f_y (MPa)	Tensile strength f_u (MPa)
Plate of SHS250×14	410	655
Corner of SHS 250×14	415	750
Beam flange (t_f = 8 mm)	400	670
Beam web (t_w = 6 mm)	405	640

The Beam-Joint-Beam (B-J-B) assembly [18] was employed for the specimen, as illustrated in Fig. 2 (a). A relatively small span of the beam l_0 = 2400 mm was used, giving a gross span-to-depth ratio of l_0/H = 8, in order to obtain the complete response of the beam-to-column connection including the damage evolution since there was a limited vertical displacement range (approximately 400 mm). The length of the central column was 1100 mm. The design of beam-column assembly was based on the strong column-weak beam seismic design philosophy according to Chinese codes [30, 31].

2.2. Test setup and instrumentation

The test specimen, mounted on a purpose-built test rig as illustrated in Fig. 2 (b), was loaded vertically at the unsupported central column by the actuator at a stroke rate less than 7 mm/min. The central column was guided at the bottom end using a sliding support so that only vertical movement of the column is possible. The two pin supports at the outer ends of the beams were designed using latch-type rollers for free rotation in the assembly plane, with their distance matching the span of 2,400 mm. The test was terminated when the connection totally lost its bearing capacity on either side.

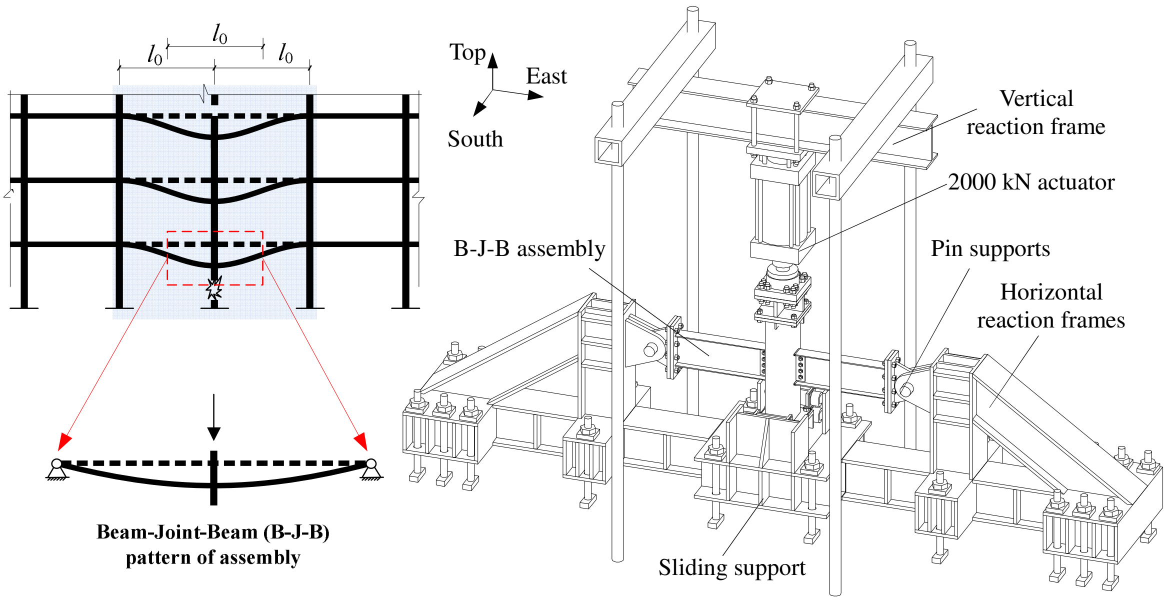

(a) B-J-B pattern [18]. (b) Components.

Fig. 2. Test setup.

Instrumentations were arranged as shown in Fig. 3 to measure the displacement of the assembly and strains at the critical regions during the test. Sixteen displacement transducers (see Fig. 3 (a)) were used to measure the assembly deflection along the beam length and any possible movements of the two pin supports. Strain gauges were arranged at six beam sections as shown in Fig. 3 (b).

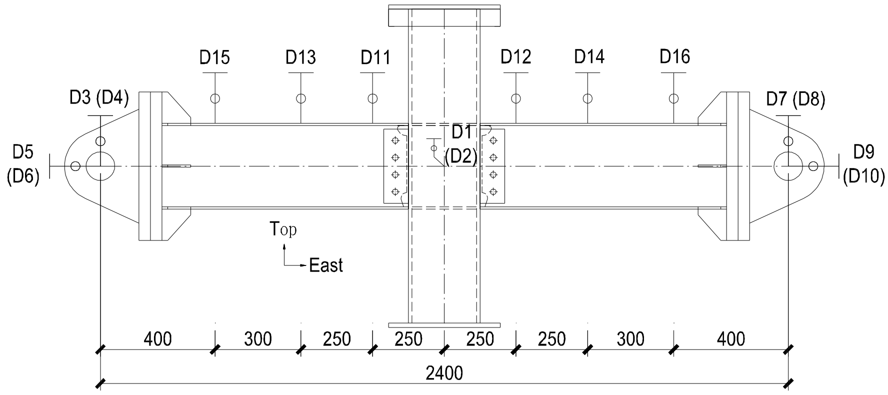

(a) Displacement transducers.

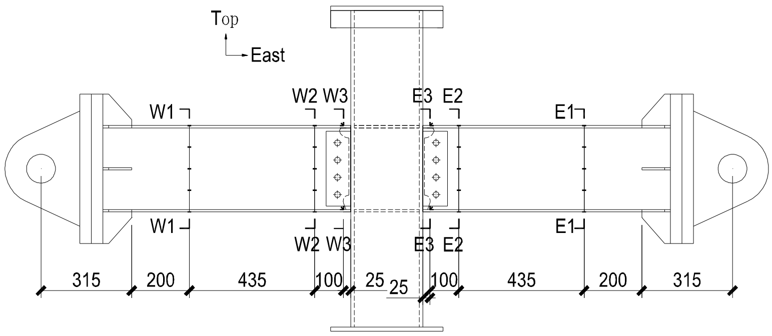

(b) Beam sections for strain gauges.

Fig. 3. Schematic arrangements of test instrumentation.

2.3. Test results

The tested specimen exhibited a complete failure process at the beam-to-column connection, where the beam on the east side totally separated from the central column. The final condition of the beam-column assembly and the detailed view of the WUF-WB connection at the end of the test are shown in Fig. 4.

The load-displacement curve of the central column is shown in Fig. 5. A few key stages are identified on the curve, and the associated damage evolutions are depicted in the corresponding photographs in Fig. 6. The nominal plastic load F_p is the vertical load causing the formation of plastic hinges at the critical locations (Sections W3 and E3), which is 359 kN. The beam chord rotation θ is obtained by dividing the vertical displacement of the central column by the distance of 1,200 mm between the column and the pin support (effectively the half-span length).

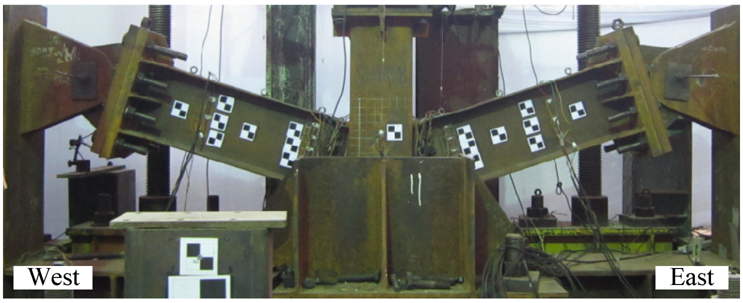

(a) Southern view of the test assembly

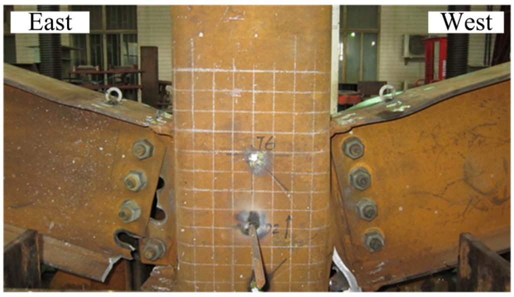

(b) Northern view of the tested WUF-WB connection

Fig. 4. Photographs of the specimen at the end of the test.

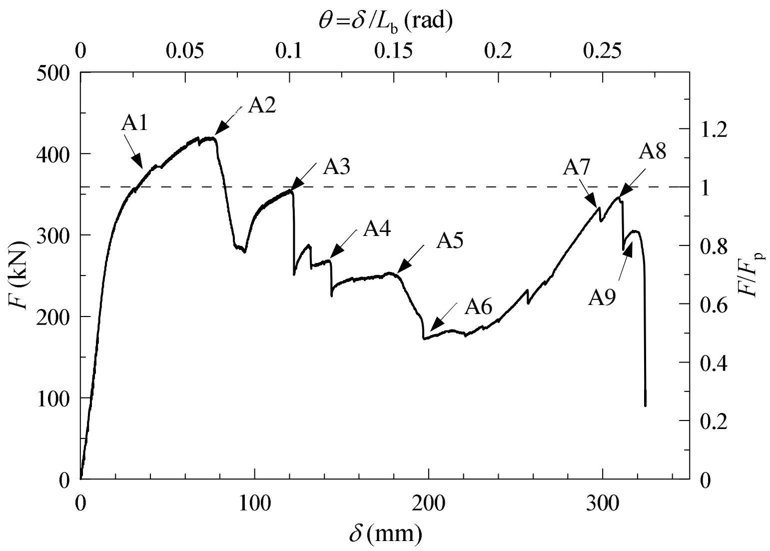

Fig. 5. Load-displacement curve of test specimen.

A1: Local buckling of top flanges near Sections W3 and E3

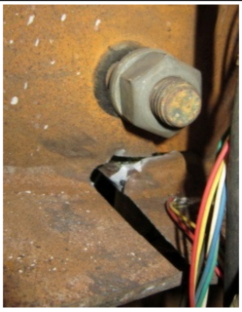

A2: Bottom flange fractured at Section E3 (1.17F_p, 0.061 rad)

A3: Column wall cracked near the southern end of bottom flange on the west side (0.99F_p, 0.100 rad)

A4: The lowest bolt was torn out of web on the east side (0.75F_p, 0.120 rad)

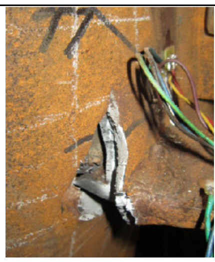

A5: Column wall cracked near the northern end of bottom flange on the west side (0.70F_p, 0.150 rad)

A6: Column wall completely fractured near the bottom flange and cracks entended upwards on the west side (0.48F_p, 0.164 rad)

A7：Shear tab fractured at the middle and top parts across the bolt holes on the east side (0.92F_p, 0.248 rad)

A8: Column wall cracked along the weld between the shear tab and column on the west side (0.96 F_p, 0.259 rad)

A9: Top flange of Section E3 fracture and the eastern beam totally separated from the column (0.84 F_p, 0.268 rad)

Fig. 6. Damage evolutions at key stages of test specimen.

As demonstrated in Fig. 5 and Fig. 6, the first significant event (point "A1" on the load-displacement curve) took place when local buckling occurred at the top flanges near Sections W3 and E3 with the displacement reaching about 40 mm, which corresponded to the beam chord rotation θ of 0.033 rad.

The applied load kept increasing until the specimen reached the first peak load (point "A2") when the bottom flange near the access hole at Section E3 fractured at a displacement of 73 mm (θ = 0.061 rad). The fracture caused a drastic drop of the applied load from the peak value of 419 kN (1.17F_p) to 281 kN (0.78F_p).

However, the flexural capacity of the beam on the other side (west side) enabled the applied load to reach a second peak value of 355 kN (0.99F_p) at a displacement of 120 mm (θ = 0.100 rad), when the column wall fractured near the southern end of the bottom flange on the west side (point "A3"), which induced an abrupt drop of load to about 250 kN (0.70F_p).

With the increasing displacement of the central column, the specimen saw two small fluctuations of the applied load from the peak value of 287 kN (0.80 F_p) at a displacement of 132 mm (θ = 0.110 rad) and from 268 kN (0.75F_p) at 144 mm (θ = 0.120 rad). In the latter event, the load suddenly reduced to about 250 kN (0.70F_p) due to the tear-out of the lowest bolt on the east side out of the web (point "A4").

When the displacement reached 180 mm (θ = 0.150 rad), the column wall fractured near the northern end of the bottom flange on the west side (point "A5"), after which the load decreased due to the crack propagation across the entire width of the bottom flange on the west side, until a complete fracture through its thickness formed below the bottom flange (point "A6"). The displacement at this point was 197 mm (θ = 0.164 rad) and the load reached the lowest value of 172 kN (0.48 F_p).

Thereafter the west-side column wall tore up from the two ends of the bottom flange as the applied load gradually recovered, on account of the development of the catenary mechanism. At a displacement of 298 mm (θ = 0.248 rad), the shear tab fractured vertically at the middle and top parts through the bolt holes on the east side (point "A7") following the horizontal crack below the third bolt, causing a slight drop in the applied load from 330 kN (0.92 F_p) to 317 kN (0.88 F_p).

The load quickly increased and reached another peak value of 345 kN (0.96 F_p) at a displacement of 311 mm (θ = 0.259 rad) when the column wall fractured along the weld connecting the shear tab and column on the west side (point "A8") with an abrupt drop of load to 280 kN (0.78 F_p). Although the load was able to slightly pick up to 303 kN (0.84 F_p), the beam-column assembly virtually lost its bearing capacity due to the complete fracture of the top flange at Section E3 and hence the separation between the eastern beam and the column (point "A9"). At this point, the displacement of central column was 321 mm (θ = 0.268 rad) and the test was terminated.

Two failure modes, the interrrupted beam-end failure mode and the column-wall failure mode [19], took place during the test. A complete process of the interrupted beam-end failure mode covering the entire damage evolution was present for the WUF-BW connection on the east side. The fracture took place initially at the bottom flange, then at the bottom of the web and the middle-top part of the shear tab, and eventually at the top flange. The fracture of the top flange signified the end of the damage evolution on this side.

On the other side (west side), the column-wall failure mode did not present a complete damage evolution, with the cracks extending upwards to one third of the beam's depth. As discussed in previous papers [19, 20], the occurrence of fracture at the column wall was preceded by the separation between the inner diaphragm and the column inside wall as shown in Fig. 7 (a).

(a) Separation on the west side.

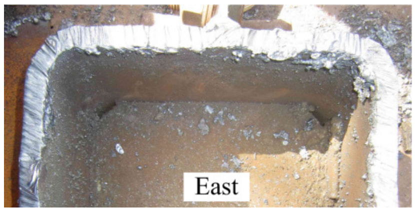

(b) Well fabricated welding on the east side.

Fig. 7. Final conditions between the bottom inner diaphragm and column inside wall.

3. Verification of numerical simulations

Numerical analyses were carried out using the explicit time integration approach in the general-purpose finite element (FE) analysis software ABAQUS [32]. The verification of the FE model was firstly made by comparing the FE simulation results against the present laboratory test results. The verified FE analysis method was subsequently used in parametric analyses for studying the performance of moment resisting beam-column assemblies under different span-to-depth ratios.

3.1. FE modelling of test specimen

The present test assembly was modelled in whole to enable the simulation of the asymmetric damage evolutions on the two sides of the WUF-BW connection. The actuator's load was simulated by a prescribed vertical displacement of the central column. The geometric, boundary and material nonlinearities including material fracture were taken account into the FE simulation. The stress-strain constitutive relationships of the steel material were defined based on the coupon test results (see Table 1).

All components were created using solid elements of the 8-node linear brick elements with reduced integration (C3D8R). In order to capture the fracture at the connection region, sufficiently fine mesh of solid elements was employed at the parts where fracture may occur, with an element size of approximately 1.0 mm, as shown in Fig. 8 (b), including the

I-section at the beam end segment together with the bolted shear tab on the east side, and the bottom inner diaphragm together with the connected column wall on the west side.

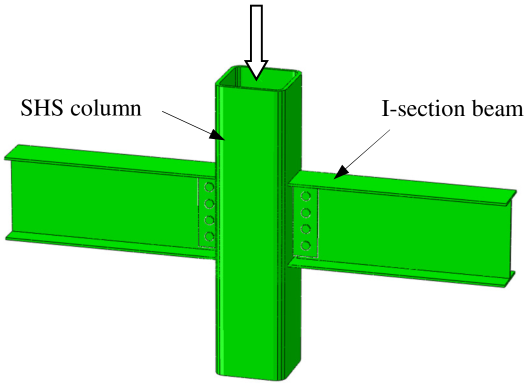

(a) FE model of the test assembly.

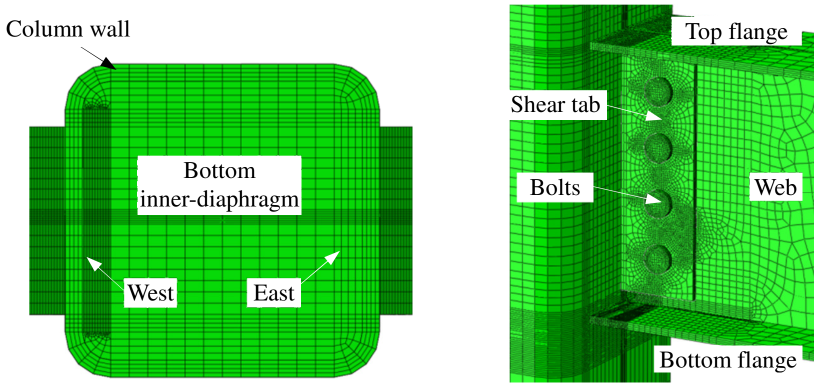

(b) Meshes in the connection region.

Fig. 8. Finite element models composed of solid elements.

The "Damage for Ductile Metals" approach was employed to activate the deletion of elements whose strain responses reach the pre-specified fracture threshold [32]. The fracture strain limits ranged from 0.2 to 0.8 for the column wall, I-section (bottom and top flanges and web) and the shear tabs surrounding the bolts. In order to simulate the column-wall failure mode on the west side, i.e. the separation between the bottom inner diaphragm and the column inside wall, the western edge of the bottom inner diaphragm was given a relatively small fracture strain limit of 0.04.

3.2. Simulation results

The final state of the test specimen in the FE simulation is shown in Fig. 9 (a), involving a beam-end interrupted failure at Section E3 on the east side and a column-wall failure on the west side. The key stages in the simulated failure process shown in Fig. 9 (b) agreed reasonably well with the experimental results presented earlier in Fig. 6, and are labelled in the same manner with respect to the fracture mode as the experimental key stages using the lower case “a” in lieu of the upper case. The numerals for the simulated key stages are not always consecutive, indicating that the sequence of fractures do not necessarily match the experimental sequence.

The FE load-displacement curve is compared against the experimental curve in Fig. 10, with the indicated key events corresponding to Fig. 6 and Fig. 9 (b). The comparison shows a reasonable agreement between the two sets of data in terms of the load development and the damage evolution.

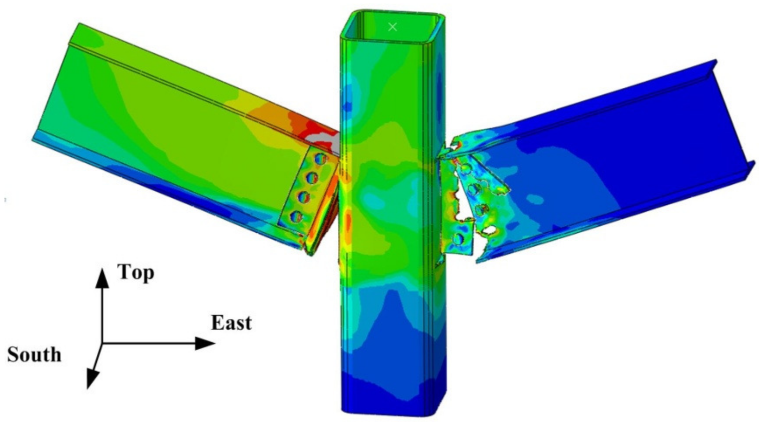

(a) Final state of the beam-column assembly.

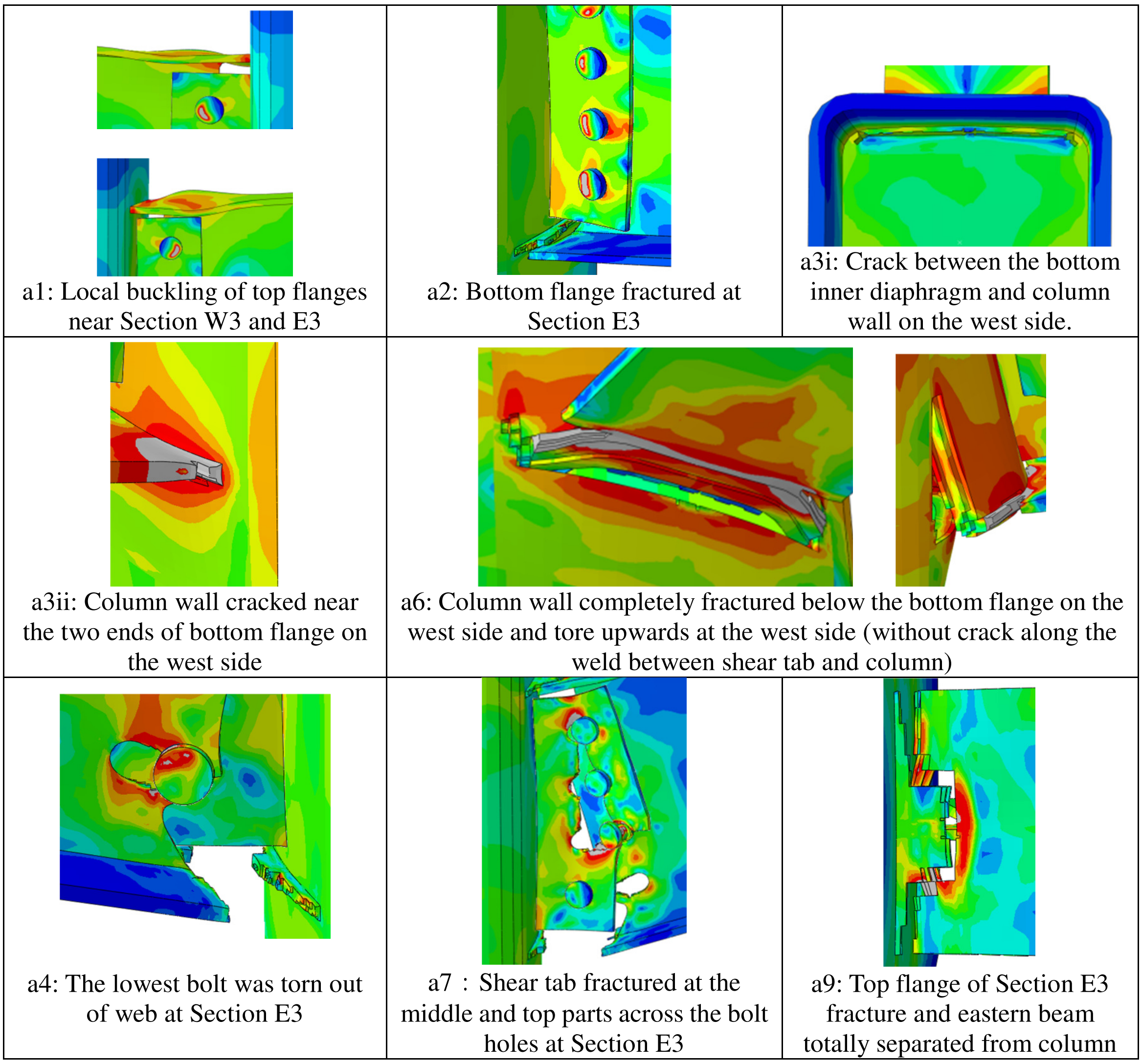

(b) Key stages in the failure process

Fig. 9. Simulated failure modes.

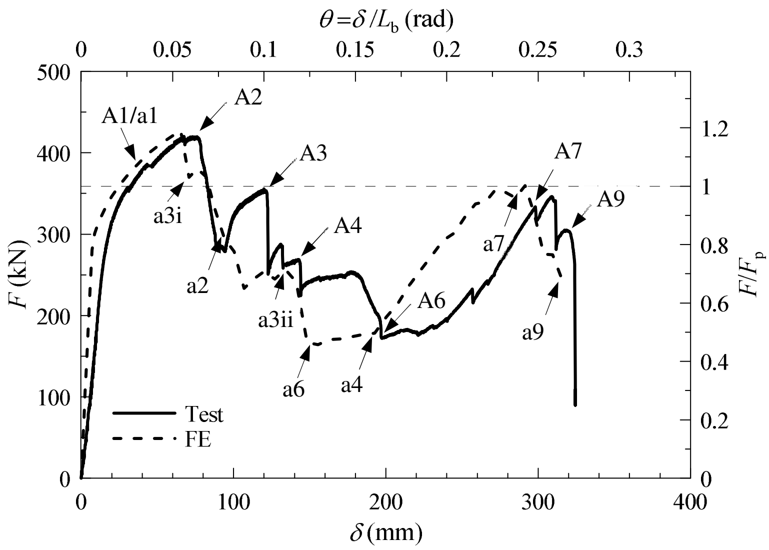

Fig. 10. Comparison of load-displacement curves between FE simulation and test for specimen.

4. Parametric analyses on span-to-depth ratios

In this section, thirty-two double-span beam-column assemblies of four different configurations shown in Table 2 were analysed under varying span-to-depth ratios. The fourth configuration in the table is the same as that of the test specimen depicted in Fig. 1. As can be seen from the table, all connections are of the WUF-BW type.

Due to symmetry, only one half of each assembly was modelled. Four span-to-depth ratios(R) of 18, 15, 12 and 8 were employed in the parametric analyses, which cover the commonly used range in design codes [33]. The beam-end interrupted failure mode and the column-wall failure mode were separately simulated (refer to Section 3.1). The label of each specimen indicates its span-to-depth ratio, failure mode ("BF" or "CF") and beam depth, in that order. The "BF" designation refers to the beam-end interrupted failure mode, and the "CF" designation refers to the column wall failure mode. For example, Specimen R18-BF-H600 is the beam-column assembly with a span-to-depth ratio R of 18, composed of beam section H600×300×12×20 connected to column section SHS 500×25 by M30×10 bolts (see Table 2), and fails by the beam-end interrupted failure mode.

Table 2. Components of four groups for beam-column assemblies in the parametric analyses.

Beam section	Column section	WUF-BW connection
H600×300×12×20	SHS 500×25	M30×10
H500×200×9×14	SHS 400×20	M24×10
H400×200×7×9	SHS 300×16	M24×8
H300×150×6×8	SHS 250×14	M20×4

4.1. Assemblies having the same span-to-depth ratio

As explained in [27], a normalized chord rotation over the plastic hinge rotation θ_p is more appropriate to use as the generalized displacement variable for the purpose of comparing the progressive collapse resistance performance between double-span moment resisting assemblies. The plastic hinge rotation θ_p is defined [27] as

$$\theta_p = \frac{\delta_p}{l_0/2} = \frac{F_p}{K_e}\frac{2}{l_0} = \frac{4W_p f_y / l_0}{48EI_b / l_0^3}\frac{2}{l_0} = \frac{W_p f_y l_0}{6EI_b} \tag{1}$$

where K_e is the elastic stiffness of a simply supported beam under a concentrated force at midspan, and I_b is the second moment of area of the beam section.

The normalized load-rotation curves of the assemblies having different beam depths but the same span-to-depth ratio are shown in Fig. 11 (a) and (b), corresponding to the beam-end interrupted failure mode and the column-wall failure mode, respectively. It can be seen that the different assemblies behave similarly to each other if their span-to-depth ratios and failure modes are the same, irrespective of their beam depths. The slight differences in the post-fracture stage of the beam-end interrupted failure mode are mostly caused by the different connection geometry (see Table 2). For the column-wall failure mode, the different capacities of the column-wall (thickness) of the assemblies relative to their respective beam section's plastic capacities may lead to some differences in their progressive collapse behaviour. However, such differences are much smaller than those between the assemblies having different span-to-depth ratios, as demonstrated in the following subsection.

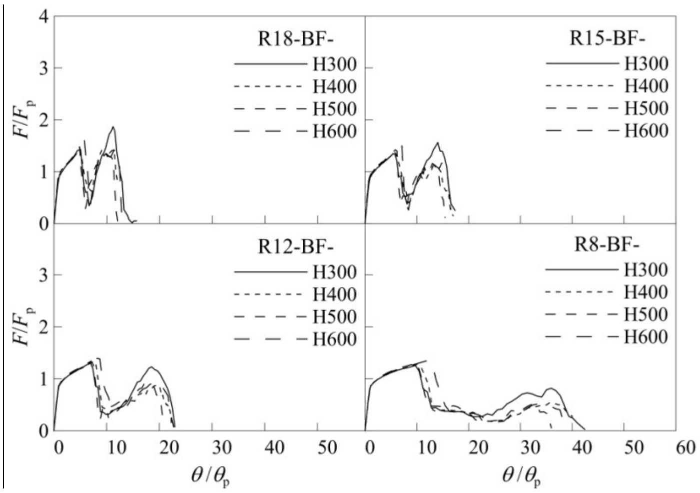

(a) Beam-end interrupted failure mode

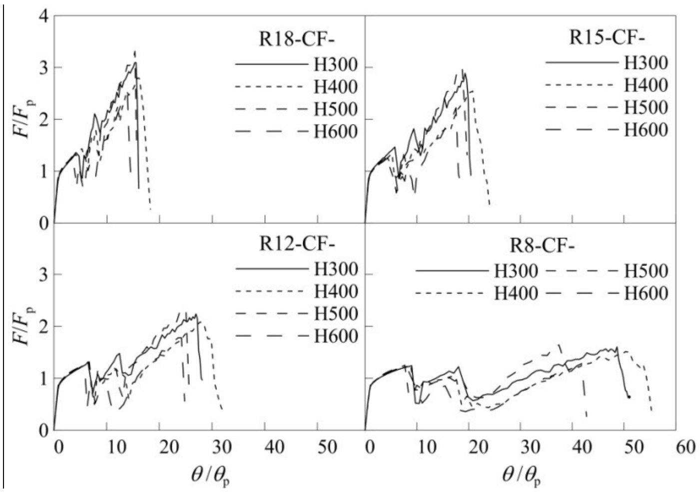

(b) Column-wall failure mode

Fig. 11. Normalized load-displacement curves for assemblies having the same span-to-depth ratio.

4.2. Assemblies having different span-to-depth ratios

In order to study the effects of span-to-depth ratio, the normalized load-rotation curves of assemblies configured with H300×150×6×8 beam under different span-to-depth ratios are compared to each other in Fig. 12 and Fig. 13, for the beam-end interrupted failure mode and the column-wall failure mode, respectively. Certain key stages of the damage evolution are identified on the curves and depicted in the accompanying figures of FE simulation. As shown in Fig. 12, each assembly experiencing the beam-end interrupted failure mode has two peak resistances associated with fractures of the bottom and the top flanges. The bottom flanges (Step “BF1” in Fig. 12) fracture when the resistances are equal to $1.25F_p$ to $1.43F_p$ at normalized chord rotations θ/θ_p ranging from 4 to 10 (at an approximately constant chord rotation of 0.07 rad), each of which is followed by a drop in the resistance to about half the plastic hinge load F_p. The resistance then recovers on account of the interaction between the bolts and the web as well as the shear tab, before it is eventually lost when the top flange factures (Step “BF2”). The second peak value of F/F_p range from 0.8 to 1.8, reached at θ/θ_p ranging from 11 to 36. The smaller the span-to-depth ratio, the lower the peak resistance and the larger the normalized rotation demand.

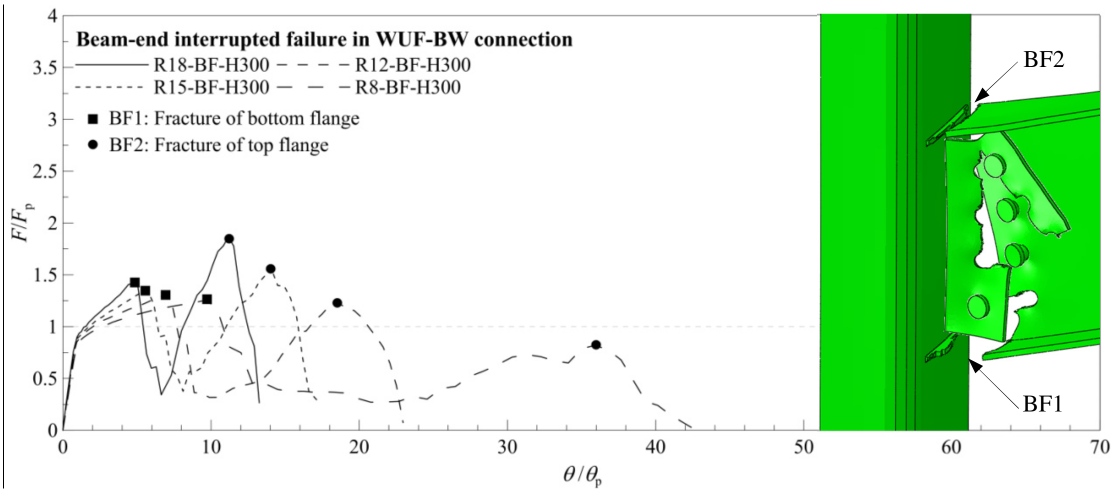

Fig. 12. Responses of assemblies having different span-to-depth ratios experiencing beam-end interrupted failure.

Fig. 13 (a) shows that, for each of the four assemblies undergoing the column-wall failure mode, the resistance quickly recovers after the first two interruptions, and the peak resistances generally exhibit an increasing trend. The first two interruptions are due to the separation between the bottom inner diaphragm and the column wall, and the fracture of the column wall, respectively, as illustrated in Fig. 13 (b). The resistance is only lost when crack takes place near the top flange. The maximum normalized resistances F/F_p range from 1.5 to 3.1, reached at θ/θ_p ranging from 16 to 49. As in the case of the assemblies undergoing the beam-end interrupted failure mode, the smaller the span-to-depth ratio, the lower the peak resistance and the larger the normalized rotation demand.

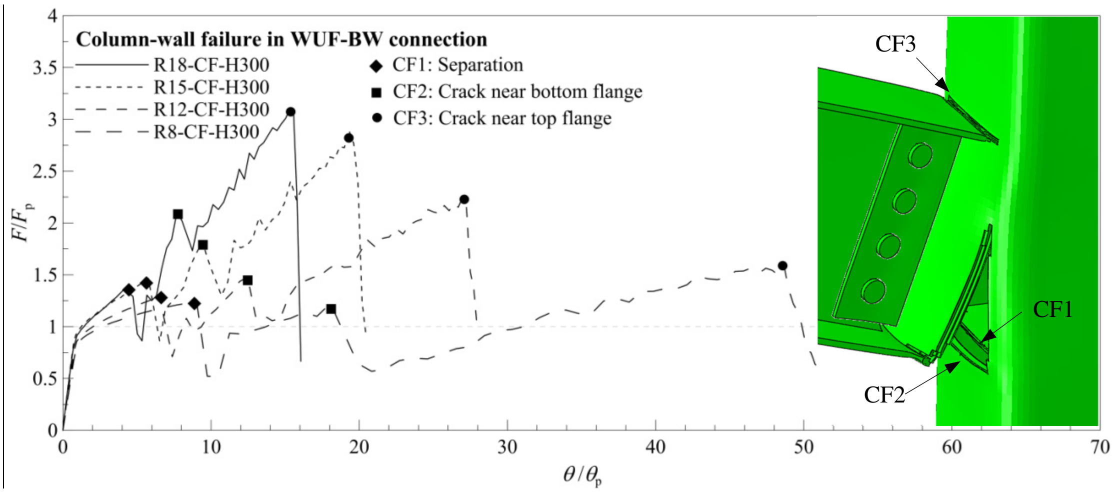

(a) Normalized load - rotation curves.

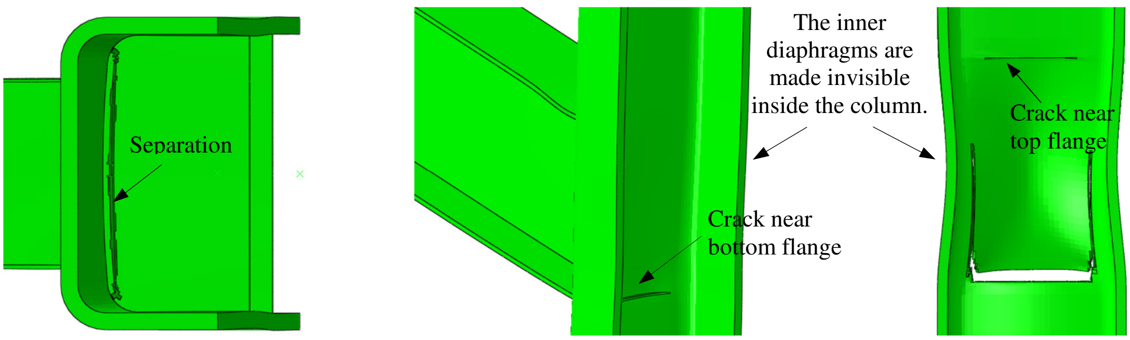

CF1: Separation between the inner diaphragm and column inside wall

CF2:Crack of the column wall near the beam bottom flange

CF3:Crack of the column wall near the top bottom flange

(b) Key stages causing resistance drops.

Fig. 13. Responses of assemblies having different span-to-depth ratios experiencing column-wall failure.

5. Flexural and catenary mechanisms under different span-to-depth ratios

Under the central column removal scenario, the gravity resistance of a moment beam-column assembly is contributed by the flexural and the catenary mechanisms. As discussed in reference [18], the vertical reaction V_R in Fig. 14, can be calculated from the following equation

$$V_R = V_i\cos\varphi_i + N_i\sin\varphi_i = F_f + F_c \tag{2}$$

where V_i, N_i and φ_i are the transverse shear force, axial force and rotation of the deflected beam section, respectively. The internal forces V_i and N_i can be determined from the strain readings located at some distances from the supports [18].

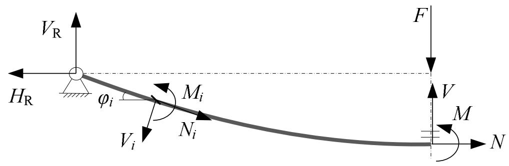

Fig. 14. Analysis of resistance and internal force for the beam-column assembly (modified from [18]).

The first term on the right hand side of Equation (2), F_f, is the resistance component due to the flexural mechanism, and the second term, F_c, is due to the catenary mechanism. The developments of these two resistance components of assemblies in Section 4.2 as computed from the equation at certain sections of the beams are shown in Fig. 15, normalized by the corresponding plastic hinge load F_p and plotted against the normalized chord rotation.

It is demonstrated in Fig. 15 (a) and (b) that the flexural resistances F_f of all assemblies develop in the same manner during the elastic stage until they exceed the plastic hinge load F_p, following which the respective initial damages (step “BF1” or “CF1”) cause drastic declines of the flexural resistances. The negative zone of each flexural resistance is due to the rapidly growing horizontal reaction force at the pin support, associated with the development of the catenary mechanism.

Fig. 15 (c) and (d) show that, although the catenary resistances F_c are affected by the early damages (step “BF1” or “CF1” and “CF2”) to drop temporarily, thereafter they increase to peak values ranging from $1.4F_\mathrm{p}$ to $3.6F_\mathrm{p}$.

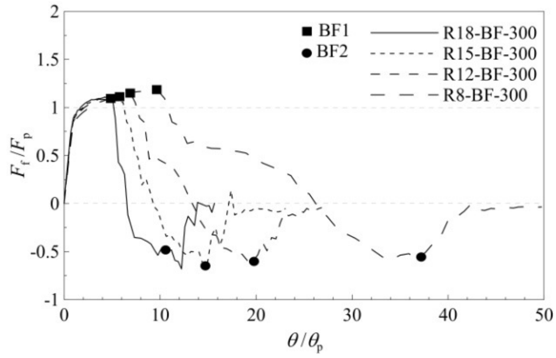

(a) Flexural mechanism for "BF" models.

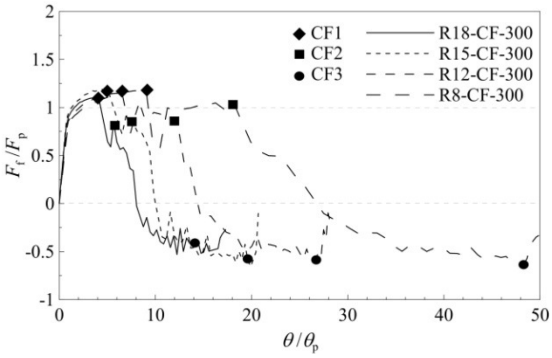

(b) Flexural mechanism for "CF" models.

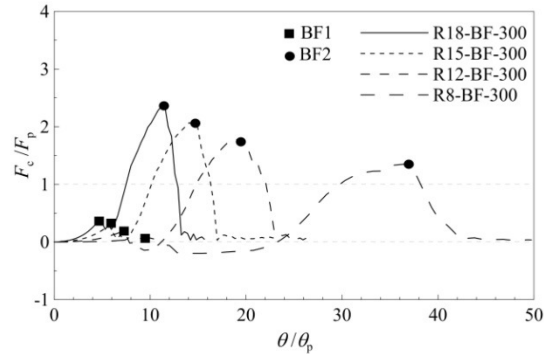

(c) Catenary mechanism for "BF" models.

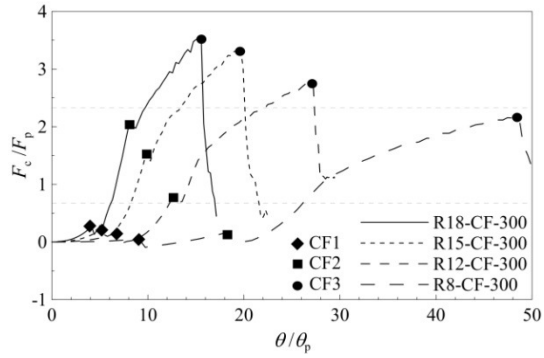

(d) Catenary mechanism for "CF" models.

Fig. 15. Developments of gravity resistances contributed by flexural and catenary mechanisms.

Based on the parametric analyses (Fig. 11, Fig. 12, Fig. 13, and Fig. 15), a schematic illustration is provided in Fig. 16 to outline the development of the progressive collapse resistance of the moment beam-column assemblies having the same beam section but two span-to-depth ratios R_1 and R_2 ($R_1 > R_2$). The two components of the gravity resistance due to the flexural and the catenary mechanisms are separately plotted in Fig. 16 (a), denoted 'f_f' and 'f_c', respectively, and their resultant is plotted in Fig. 16 (b). Three distinctive stages are identified as indicated in the graphs, being the flexure dominated stage "I", the combined flexure-catenary stage "II" and the catenary dominated stage "III". The three stages are separated from each other by the plastic hinge formation and the initial fracture of the connection (such as "BF1" and "CF1" when $\theta/\theta_p = \gamma_{if1}$ or γ_{if2}). Stage "III" ends when the last fracture takes place in the connection (such as "BF2" and "CF3" when $\theta/\theta_p = \gamma_{uf1}$ or γ_{uf2}).

It can be seen that the assembly with a larger span-to-depth ratio R_1 is able to provide a higher ultimate gravity resistance ratio η_{u1} due to its more effective facilitation of the catenary mechanism. However, the smaller span-to-depth ratio R_2 enables the assembly to resist the ultimate load at a greater chord rotation ratio γ_{u2}.

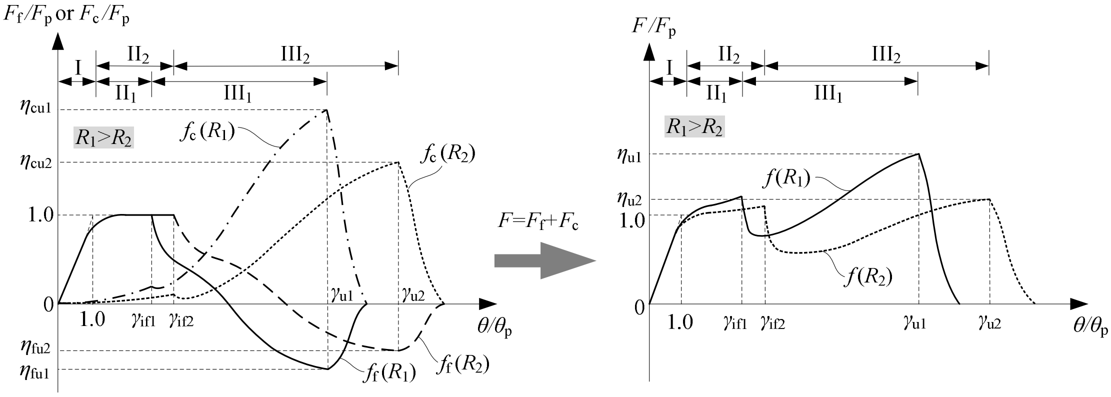

(a) Flexural and catenary resistances (b) Total gravity resistance

Fig. 16. Schematic illustration of gravity resistance development for beam-column assembly.

For a convenient assessment of the beam-column assembly directly affected by the removed column [23], a simplified curve for the gravity resistance development is proposed in Fig. 17. It is suitable for the connection methods exhibiting failure modes that facilitate an effective development of the catenary mechanism in the post-fracture stage, such as the beam-end interrupted failure mode and the column-wall failure mode. The assembly has a gravity resistance of F_p when a plastic hinge forms at the beam-end section at chord rotation θ_p (refer to equation (1)). Afterwards, the gravity resistance grows to $\eta_{if}F_p$ (at a slower rate) until the initial fracture occurs at chord rotation $\eta_{if}\theta_p$, which causes a loss of gravity resistance equal to $\Delta\eta_{if}F_p$. The gravity resistance may then plateau, a response which is most pronounced for the assembly having a small span-to-depth ratio undergoing the beam-end interrupted mode (see Fig. 12), and which can be neglected otherwise. The assembly reaches the ultimate gravity resistance η_uF_p when the damage has extended upwards close to the top flange, with corresponding chord rotation of $\gamma_u\theta_p$, after which the gravity resistance is deemed to be lost completely.

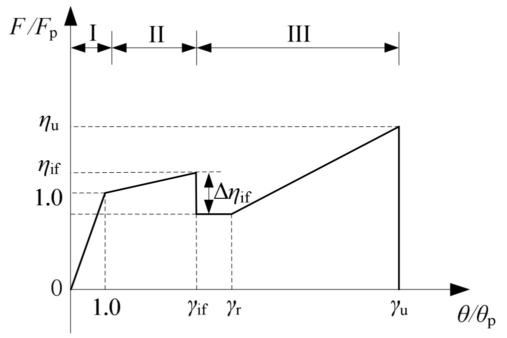

Fig. 17. Simplified curve model for the development of gravity resistance.

The values of the parameters in the proposed simplified curve model in Fig. 17, including the gravity resistance ratios and the chord rotation ratios, depend on the span-to-depth ratio and connection methods as well as the failure modes. Further research is required to quantify them.

6. Conclusions

The full response of moment resisting beam-column assemblies, extracted from the bays directly affected by a failed interior column in a typical steel framing system, have been investigated under different span-to-depth ratios covering the commonly used range through an experimental test and thirty-three numerical simulations.

The tested specimen, a B-J-B assembly with a beam span-to-depth ratio of 8, experienced failures at the beam-end section and in the column wall on the two sides of the WUF-BW connection, respectively. Both the beam-end interrupted failure mode and the column-wall failure mode enabled the assembly to effectively facilitate the development of the catenary mechanism in the post-fracture stage, which is important for structure bridging over a failed interior column so as to prevent progressive collapse.

Parametric analyses of beam-column assemblies having four span-to-depth ratios (18, 15, 12 and 8) have been conducted, using validated finite element (FE) models which took account of material fracture. It has been demonstrated that assemblies having the same span-to-depth ratio behave similarly in terms of their normalized load-rotation relationships even though they are configured with different beam depths. Conversely, assemblies having the same beam and column sections but different span-to-depth ratios behave differently in terms of their normalized load-rotation relationships.

Nevertheless, for a particular failure mode of the moment connection that is capable of facilitating an effective development of the catenary mechanism, the gravity resistance developments of all assemblies share a common trend despite their different span-to-depth ratios (and different beam sections). The three development stages, being the flexure dominated stage, the combined flexure-catenary stage and the catenary dominated stage, are separated from each other by the plastic hinge formation at the critical beam section and the initial fracture in the connection region.

In general, the beam-column assembly with a larger span-to-depth ratio is able to develop the gravity resistance earlier, and provide a higher ultimate resistance by facilitating a more effective catenary mechanism. However, the assembly with a smaller span-to-depth ratio exhibits a more ductile response.

A simplified curve model of the gravity resistance development of a moment beam-column assembly with damage evolution has been proposed for a convenient assessment of the progressive collapse resistance following a central column loss. Further research is required to quantify the model parameters.

Acknowledgments

The research presented in this paper was supported by the Natural Science Foundation of China (NSFC) through No. 51008220 and 51378380. Any opinions, findings, conclusions, and recommendations expressed in this paper are those of the authors and do not necessarily reflect the views of the sponsors.

References

[1] Japanese Society of Steel Construction Council on Tall Buildings and Urban Habitat. Guidelines for collapse control design construction of steel buildings with high redundancy. Tokyo: The Japan Iron and Steel Federation; 2005.

[2] Department of Defense: Design of buildings to resist progressive collapse.Washington, D.C.: Department of Defense; 2009 [UFC 4-023-03].

[3] General Service Administration: Progressive collapse analysis and design guidelines for new federal office buildings and major modernization projects. Washington, D.C.: General Service Administration; 2003.

[4] Ellingwood BR, Leyendecker VE. Approaches for design against progressive collapse. *Journal of the Structural Division ASCE*. 1978;104(3):413–423.

[5] Ellingwood BR, Smilowitz R, Dusenberry DO, Duthinh D, Lew HS, Carino NJ. Best practices for reducing the potential for progressive collapse in buildings. Rep.No. NISTIR 7396. Maryland: National Institute of Standards and Technology; 2007.

[6] Yi WJ, He QF, Xiao Y, Kunnath SK. Experimental study on progressive collapse-resistant behavior of reinforced concrete frame structures. *ACI Structural Journal.* 2008;105(4): 433–439.

[7] Astaneh-Asl A, Jones B, Zhao Y. Progressive collapse resistance of steel building floors. Rep. No. UCB/CEE-STEEL-2001/03. University of California at Berkeley; 2001.

[8] Demonceau JF, Jaspart JP. Experimental test simulating a column loss in a composite frame. *Advanced Steel Construction*. 2010;6(3):891–913.

[9] Sasani M, Kazemi A, Sagiroglu S, Forest S. Progressive Collapse Resistance of an Actual 11-Story Structure Subjected to Severe Initial Damage. *ASCE Journal of Structural Engineering*. 2011;137:893-902.

[10] Stylianidis PM, Nethercot DA. Modelling of connection behaviour for progressive collapse analysis. *Journal of Constructional Steel Research*. 2015;113:169-84.

[11] Karns JE, Houghton DL, Hong JK, Kim J. Behaviour of varied steel frame connection types subjected to air blast, debris impact, and/or post-blast progressive collapse load conditions. *Structures Congress 2009*. 2009; 1868-1877 [Austin].

[12] Lew HS, Main JA, Robert SD, Sadek F, Chiarito VP. Performance of Steel Moment Connections under a Column Removal Scenario. I: Experiments. *ASCE Journal of Structural Engineering*. 2012; 139(1): 98-107.

[13] Kozlowski A, Gizejowski M, Sleczka L, Pisarek Z, Saleh B. Experimental investigations of the joint behavior-robustness assessment of steel and steel-concrete composite frame. In: Nunai L, Iványi M, Jármai K, editors. *Proceeding of 6th conference on steel and composite structures*; 2011 [Hungary, Budapest].

[14] Lew HS, Bao YH, Sadek F, Main JA, Pujol S, Sozen MA. An experimental and computational study of reinforced concrete assemblies under a column removal scenario, Rep. No. NIST Technical Note 1720.

Maryland: National Institute of Standards and Technology; 2011.
[15] Sadek F, Main JA, Lew HS, Robert SD, Chiarito VP, El-Tawil S. An experimental and computational study of steel moment connections under a column removal scenario. Rep. No. NIST Technical Note 1669. Maryland: National Institute of Standards and Technology; 2010.
[16] Yang B, Tan KH. Experimental tests of different types of bolted steel beam–column joints under a central-column-removal scenario. *Engineering Structure.* 2013;54:112–130.
[17] Guo L, Gao S, Fu F. Structural performance of semi-rigid composite frame under column loss. *Engineering Structures*. 2015;95:112-26.
[18] Li L, Wang W, Chen YY, Lu Y. Experimental investigation of beam-to-tubular column moment connections under column removal scenario. *Journal of Constructional Steel Research*. 2013; 88: 244–255.
[19] Li L, Wang W, Chen YY, Lu Y. Effect of beam web bolt arrangement on catenary behaviour of moment connections. *Journal of Constructional Steel Research.* 2015; 104: 22-36.
[20] Li L, Wang W, Chen YY, Teh LH. Column-wall failure mode of steel moment connection with inner diaphragm and catenary mechanism. *Engineering Structures*. 2016; 131: 553-563.
[21] Qin X, Wang W, Chen YY, Bao YH. Experimental study of through diaphragm connection types under a column removal scenario. *Journal of Constructional Steel Research.* 2015; 112: 293-304.
[22] Qin X, Wang W, Chen Y, Bao Y. A special reinforcing technique to improve resistance of beam-to-tubular column connections for progressive collapse prevention. *Engineering Structures*. 2016;117:26-39.
[23] Izzuddin BA, Vlassis AG, Elghazouli AY, Nethercot DA. Progressive collapse of multi-storey buildings due to sudden column loss - Part I: Simplified assessment framework. *Engineering Structures*. 2008;30:1308-18.
[24] Lee C-H, Kim S, Lee K. Parallel axial-flexural hinge model for nonlinear dynamic progressive collapse analysis of welded steel moment frames. *ASCE Journal of Structure Engineering ASCE.* 2010;136(2):165–173.
[25] Rezvani FH, Yousefi AM, Ronagh HR. Effect of span length on progressive collapse behaviour of steel moment resisting frames. *Structures*. 2015;3:81-89.
[26] Weigand JM, Berman JW, Integrity of Steel Single Plate Shear Connections Subjected to Simulated Column Removal. *ASCE Journal of Structural Engineering*, 2014. **140**(5): 04013114.
[27] Li L, Wang W, Chen YY, Teh LH. A basis for comparing progressive collapse resistance of moment frames and connections. *Journal of Constructional Steel Research*. Under review.
[28] Architecture Institute of Japan. Technical recommendations for steel construction for buildings—part 1 guide to steel–rib fabrications. Tokyo: Architecture Institute of Japan; 1996.
[29] Ministry of Construction of China. Code for design, construction and acceptance of high strength bolting for steel structure. Beijing: China Architecture & Building Press; 1992 [JGJ 82-91].
[30] Ministry of Construction of China: Code for design of steel structures. Beijing: China Architecture & Building Press; 2003 [GB 50017-2003].
[31] Ministry of Construction of china: Code for seismic design of buildings. Beijing: China Architecture & Building Press; 2010 [GB 50011-2010].
[32] ABAQUS analysis user's manual version 6.7. ABAQUS Inc; 2007.
[33] Ministry of Construction of China: Techincal specification for concrete structures of tall building. Beijing: China Architecture & Building Press; 2002 [JGJ3-2010].

List of figures

List of tables